ACS APPLIED MATERIALS & INTERFACES

Research Article

www.acsami.org

# Effect of the Preparation Procedure on the Morphology of Thin $TiO_2$ Films and Their Device Performance in Small-Molecule Bilayer Hybrid Solar Cells

Eva L. Unger,[†,∇] Francesca Spadavecchia,[‡] Kazuteru Nonomura,[†,∇] Pål Palmgren,[§,∇] Giuseppe Cappelletti,[‡] Anders Hagfeldt,[†] Erik M. J. Johansson,[†] and Gerrit Boschloo*[,†]

[†]Department of Chemistry—Ångström Laboratory, Uppsala University, Box 523, 75120 Uppsala, Sweden

[‡]Dipartimento di Chimica, Università degli Studi di Milano, Via Golgi 19, 20133 Milano, Italy

[§]Department of Physics and Astronomy, Molecular and Condensed Matter Physics, Uppsala University, Box 530, 752 21 Uppsala, Sweden

Supporting Information

**ABSTRACT:** Flat titanium dioxide films, to be used as the acceptor layer in bilayer hybrid solar cell devices, were prepared by spray-pyrolysis and by spin-casting. Both preparation methods resulted in anatase titania films with similar optical and electronic properties but considerably different film morphologies. Spray pyrolysis resulted in dense $TiO_2$ films grown onto and affected by the surface roughness of the underlying conducting glass substrates. The spin-casting preparation procedure resulted in nanoporous titania films. Hybrid solar cell devices with varying layer thickness of the small-molecule semiconducting dye TDCV-TPA were investigated. Devices built with spray-pyrolyzed titania substrates yielded conversion efficiencies up to 0.47%. Spin-cast titania substrates exhibited short circuits for thin dye layer thickness. For thicker dye layers the performance of these devices was up to 0.6% due to the higher interfacial area for charge separation of these nanoporous $TiO_2$ substrates.

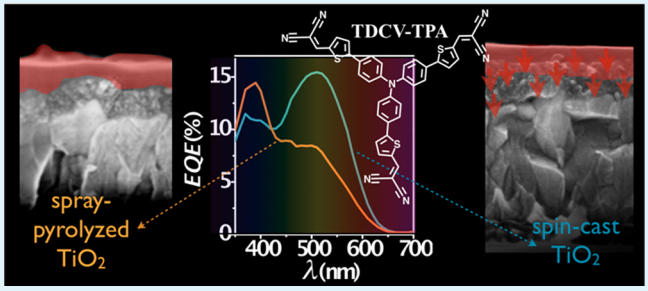


**KEYWORDS:** *hybrid solar cells, titanium dioxide, spray-pyrolysis, spin-casting, small-molecule semiconductor*

## 1. INTRODUCTION

In hybrid solar cells (HSCs), the opto-electronic properties of inorganic and organic semiconducting materials are combined to convert sunlight into electricity.[1,2] Conceptually, HSCs are related to both dye-sensitized solar cells (DSCs) and organic solar cells (OSCs), which are both technologies with the potential to become low-cost alternatives to solely inorganic photovoltaic devices.

Because of their high electron affinity and the possibility to prepare defined nanostructures, inorganic semiconductors such as $TiO_2$ and ZnO have been used as electron acceptor materials in HSC devices.[3−10] In HSCs incorporating these wide-bandgap semiconductors, photons are predominantly harvested in the organic component of the device, where excitons are formed upon light absorption. Excitons generated within the exciton diffusion length ($L_{XD}$) from the hetero interface can contribute to the photocurrent.[11] After interfacial charge carrier separation, electrons and holes must be transported to their respective contacts in the device architecture. The interfacial area between the inorganic and organic semiconductor thus governs the maximum generated photocurrent.[15] In addition to acting as the electron acceptor, the layer of wide-bandgap inorganic semiconductors also prevents recombination.[3,12−14]

Bilayer HSCs utilizing planar $TiO_2$ layers as inorganic component and polymers or small-molecule semiconductors as organic component typically have power conversion efficiencies between 0.1% and 0.5%.[8−10,16−20] Flat $TiO_2$ layers for bilayer HSCs have been prepared by spray-pyrolysis,[10,20] chemical vapor deposition (CVD),[8,9] and spin-casting of $TiO_2$ precursors.[8,9,16,17,21] In this study, we have compared titania films prepared both via spray pyrolysis[20,22] and via a spin-casting sol−gel procedure.[8,23] We demonstrate that the different preparation routes lead to anatase titania films with significantly different morphology.

Bilayer solar cell devices, using the small-molecule semiconductor TDCV-TPA (shown in the inset of Figure 3, shown later in this paper) were investigated using both types of prepared titania substrates. This compound was developed by Roncali and co-workers as a small-molecule donor in an organic solar cell.[24,25] We have demonstrated promising efficiencies using TDCV-TPA in hybrid bilayer solar cells.[20] The realization of efficient HSC devices based on the infiltration of

Received: August 14, 2012
Accepted: October 15, 2012
Published: October 15, 2012

  

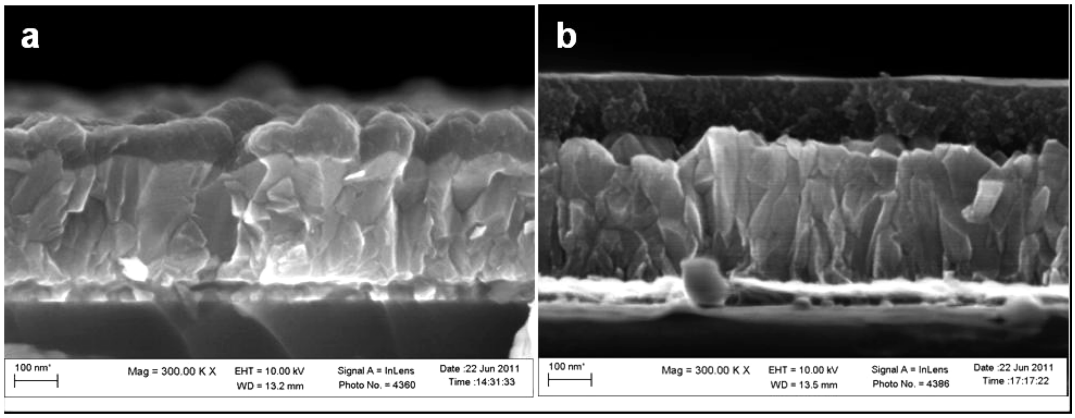


**Figure 1.** Cross-sectional scanning electron microscopy (SEM) images of (a) spray-pyrolyzed $TiO_2$ on FTO and (b) spin-coated sol–gel $TiO_2$ on FTO.

nanostructured inorganic semiconductors might be hampered by insufficient pore infiltration of organic polymer semiconductors.[26] In previous work, we found that the molecular weight of an organic semiconductor affects the pore filling fraction in nanostructured polymer/titania samples.[27] Therefore, we focus our work on the investigation of small-molecule organic semiconductors that should have a similar pore filling ability of mesoporous $TiO_2$ as the organic hole transporting material spiro-MeOTAD, commonly used in solid-state DSC.[3]

The bilayer solar cell devices built with both types of substrates exhibited very different characteristics and performance. The spray-pyrolyzed $TiO_2$ films exhibited trends observed previously[20] but the device performance achieved herein was higher (0.47%). Spin-casting $TiO_2$ films from a sol–gel solution onto conducting FTO substrates resulted in films that exhibited nanoporosity which resulted in device failure for thin layers of $TiO_2$ but also in devices outperforming the spray-pyrolyzed films for thicker dye layers. These results compare favorably with other bilayer HSC devices (0.60%).[8−10,16−20]

## 2. EXPERIMENTAL SECTION

Thin layers of titania on conducting fluorine-doped tin oxide (FTO) glass substrates (TEC15, Pilkington, substrate thickness = 2.3 mm) were prepared either by spray pyrolysis[20,22] or by spin-casting.[8,23] Preparation via spray pyrolysis was carried out as reported previously, using a titanium diisopropoxide–bisacetylacetonate $TiO_2$ precursor in 12 spray cycles, using a hand-held airbrush at 450 °C.[20] The spin-casting deposition of sol–gel $TiO_2$ films was carried out in a manner similar to routes described in the literature[8,23] from a precursor solution containing 1.4 mL of titanium-tetraisopropoxide (Aldrich), 8 mL of an ethanol, and small quantities of deionized (DI) water and hydrochloric acid (HCl, Aldrich).[8] The sol–gel solution (20 $\mu L/cm^2$) was spin-cast onto FTO substrates at 2000 rpm (Chemat Technology KW-4A spin-coater), left to condense at 120 °C (12 h), and calcined at 450 °C on a hot plate for 30 min.

Room-temperature X-ray diffraction (XRD) was measured on a Siemens Diffractometer D5000. Scanning electron microscopy (SEM) images were recorded on a Zeiss Leo 1550 SEM device. The thickness of the deposited titania films and film morphology was evaluated from SEM cross-sectional images. Atomic force microscopy (AFM) measurements were performed in tapping mode on a NanoScope III, using a silicon cantilever, which had a tip radius of better than 10 nm. Image analysis was carried out using Nanotec WSxM 5.0 software.[28] The transmittance and reflectance of the prepared titania films were measured on a Cary 5000 spectrometer equipped with an integrating sphere.

Experimental details on electrochemical measurements performed on the deposited $TiO_2$ films can be found in the electronic Supporting Information (ESI). Photoelectron spectroscopy (PES) measurements were performed using synchrotron light at the undulator-based BL I411 at the Swedish national laboratory MAX in Lund.[29,30] The takeoff angle used was 70°, and the angle between polarization and photoelectron direction was 0°. The photon energy used in the PES experiments was 100 eV.

The small-molecule semiconducting dye [tris(dicyano-vinyl-2-thienyl)phenyl]amine (TDCV-TPA, structure shown in Figure 3, presented later in this work) was purchased from Aldrich and used as-received. The dye was spin-cast (30 s, 4000 rpm) from a methylene-chloride (Aldrich) solution, as described previously,[20] and dye layers of varying thickness were prepared from different solution concentrations. The dye layer thickness ($d$) was estimated from the sample absorbance ($A$), as measured with an Ocean Optics Model HR2000 fiberoptic spectrometer. The correlation factor ($\alpha'$) was determined by relating the measured absorbance of dye layers on glass substrates with the thickness determined by step profilometry on a DekTak 150. The devices were contacted with a spin-cast layer of poly(3,4-ethyl-enedioxy-thiophene):poly-(styrene-sulfonate) (PEDOT:PSS, Aldrich) and compressed graphite powder as described previously.[20] During characterization, a mask with the same area as the active area of the test devices (0.19 $cm^2$) was used.

Current–voltage ($J$–$V$) measurements were carried out using a solar simulator (Newport, Model 91160) in combination with a computer-controlled Keithley 2400 source meter in ambient atmosphere. External quantum efficiency (EQE) values were measured under illumination from a xenon light source (ASB-XE-175) and a computer-controlled monochromator (AB301-T) with a Keithley multimeter (Model 2700). Open-circuit photovoltage ($V_{OC}$) decay measurements were carried out on a computer-controlled white LED, in combination with a DAQ multimeter used to read out the voltage decay of a solar cell device after turning off the illumination source.

## 3. RESULTS AND DISCUSSION

**3.1. Morphological and Electronic Properties of the $TiO_2$ Films.** Various experimental methods (SEM, AFM, XRD, PES, UV–vis with an integrating sphere, linear scanning voltammetry, and Mott–Schottky measurements) were employed to characterize the differences between the titania films prepared using the different preparation routes. We herein summarize the most prominent differences. The interested reader is referred to the ESI for more details on these experimental results.

The titania samples prepared by spray-pyrolysis in 12 spray cycles had an even, faint yellowish color, which stems from interference effects for the thin titania films on FTO. Spin-casting resulted in films with even coloring throughout most of the film. Figure 1 compares the cross-sectional SEM images of

the spray-pyrolyzed $TiO_2$ (Figure 1a) and spin-cast $TiO_2$ (Figure 1b). SEM images of the sample surfaces can be found in the ESI. Comparing the SEM cross-sectional images, the spray-pyrolyzed and spin-cast $TiO_2$ films have a rather dissimilar appearance.

The spray-pyrolyzed $TiO_2$ film (the slightly darker shade of gray in Figure 1a) grows on the underlying FTO and forms an intimate contact. From the SEM and AFM images (see the ESI) of the FTO surface, it is evident that the fluorine-doped tin oxide substrate consists of large crystallites with sharp edges. Both in the SEM image of the cross-section and in the image of the sample surface (see the ESI), the spray-pyrolyzed $TiO_2$ film seems to be rounding off the sharp edges of the FTO surface by adapting to the surface topography of the FTO layer.

In contrast, the spin-cast $TiO_2$ film appears more like a separate layer lying on top of the FTO and the sharp edges of the surface of the FTO substrate are visible. The thickness ($t$) of the deposited $TiO_2$ layers were determined from these SEM cross-section images and are summarized in Table 1. The

**Table 1. Film Morphology of Spray-Pyrolyzed and Spin-Cast $TiO_2$**

| sample | $B^a$ (nm) | $t^b$ (nm) | $R_{rms}{}^c$ (nm) | $h_{av}{}^c$ (nm) |
|---|---|---|---|---|
| spray-$TiO_2$ | 26 | 85 (±20) | 16.2 | 53.7 |
| spin-$TiO_2$ | 25 | 130 (±20) | 4.2 | 11.4 |
| FTO | | 330 | 29.1 | 79.4 |

[a]Crystallite size determined from XRD (200) peak (see ESI). [b]$t$ = film thickness of $TiO_2$ and FTO layers, determined from cross-sectional SEM analysis. [c]Root-mean-surface roughness $R_{rms}$ and average height $h_{av}$, determined from AFM surface analysis.

surface of the spin-cast $TiO_2$ (Figure 1b) film is more smooth, compared to the spray-pyrolyzed $TiO_2$ film (Figure 1a) which adapts to the surface roughness of the underlying FTO substrate.

The two different types of prepared $TiO_2$ films were also analyzed using AFM. The AFM images are compared in Figure 2. For both samples, the underlying FTO crystals are apparent as larger domains on the order of 150−300 nm (see the ESI). From the analysis of the AFM images, the average height ($h_{av}$) and the root-mean square surface roughness ($R_{rms}$) of the titania films were determined and are included in Table 1. In comparison to the $R_{rms}$ of the FTO substrate (Table 1), the $TiO_2$ layer deposited by spray pyrolysis decreases the surface roughness by a factor of 1.7. $TiO_2$ films prepared by the spin-casting route have a lower $R_{rms}$ and have, as also is apparent in the SEM cross-section images (Figure 1b), a smoother surface.

While AFM gives valuable information on the surface topography of a sample, the experimental results give little information about the porosity of a sample. What we can deduce is that, for both the spin-cast and spray-pyrolyzed $TiO_2$ films, small particles on the order of 20 nm are distinguishable in the AFM and SEM image. In XRD analysis, both types of samples were found to be anatase $TiO_2$ (see the ESI). From the XRD analysis, the crystallite size ($B$) was determined using the Scherrer equation. Both types of $TiO_2$ were found to contain crystallites on the order of 25 nm, and the values are included in Table 1. From the AFM and SEM images, it seems that, for the spray-pyrolyzed $TiO_2$ films, these crystallites build up the titania films in a densely fused manner, while, for the spin-cast $TiO_2$ films, the crystallites are more loosely connected. We infer that these films are nanoporous.

The differences in the $TiO_2$ film morphology is a consequence of the different conditions in the preparation routes employed. Spray-pyrolysis deposition results in compact $TiO_2$ films grown layer by layer adapting to the surface morphology. In the spin-casting preparation route titania crystallites are likely to form during storage at 120 °C of the gel film. Small $TiO_x$ crystallites form, which are subsequently fused together during sintering at 450 °C. The resulting titania films consist of $TiO_2$ nanocrystallites, forming a nanoporous structure.

For the solar cell devices investigated herein, the relative energetic alignment between the excited state of the dye and the $TiO_2$ conduction band determines the charge separation efficiency of the solar cell devices. It is, therefore, of interest to establish whether the different preparation methods have an influence on the electronic properties of the resulting titania films.

The valence band structure of the prepared titania samples could be directly investigated with photoelectron spectroscopy (PES) measurements, using synchrotron radiation (see the ESI). The valence-band edge ($E_V$) was measured to be at 3.2 eV, relative to the Fermi level ($E_F$) in $TiO_2$ and was found to be similar for both types of titania films.

Transmittance ($T$) and reflectance ($R$) measurements were carried out on an ultraviolet−visible light (UV-vis) spectrometer equipped with an integrating sphere (see the ESI). The

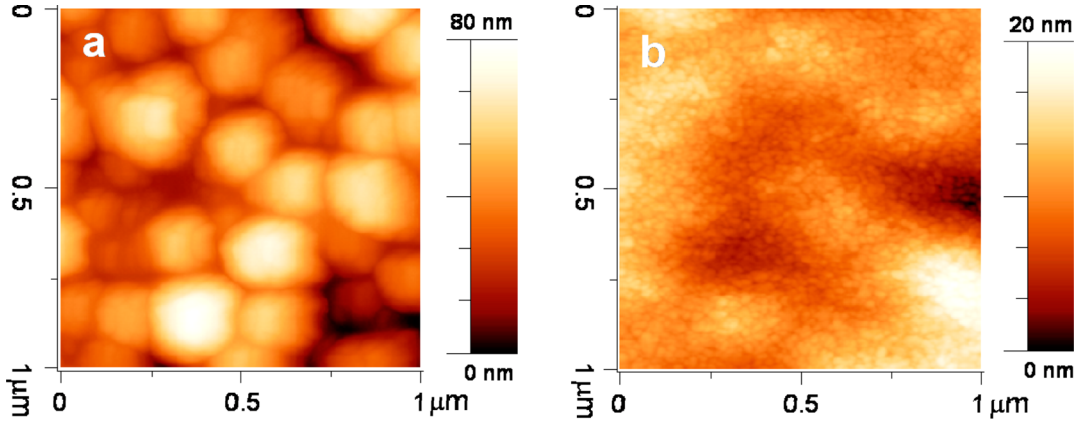


**Figure 2.** Atomic force microscopy (AFM) micrographs of the surface morphology of (a) spray-pyrolyzed and (b) spin-coated $TiO_2$ on FTO glass substrates. Note the difference in magnitude for the two $z$-scales.

indirect bandgap ($E_g$) of the titania samples was determined from the plot of $(\alpha h\nu)^{1/2}$ vs photon energy ($h\nu$) and was found to be 3.4 eV for the spin-cast $TiO_2$ and 3.35 eV for the spray-pyrolyzed $TiO_2$. This is comparable to values previously reported for titania films consisting of nanoparticles.[31]

In order to investigate the conduction band of the prepared titania samples, we attempted to determine the flat band potential ($V_{fb}$) from the Mott–Schottky plot of the space charge capacitance ($C_{SC}$). While we were able to determine the $V_{fb}$ value of the spray-pyrolyzed $TiO_2$ samples to be −0.26 V vs NHE at pH3 (see the ESI), in agreement with values previously reported,[32,33] we were not able to measure the $V_{fb}$ value of spin-cast $TiO_2$ films on FTO. This was a consequence of the films exhibiting pinholes and, therefore, not blocking electron transfer with the underlying FTO layer. This was confirmed in linear scan voltammetry experiments using ferrocene, which also can be found in the ESI. Although these experiments did not allow us to compare the flatband potentials of the two different types of titania films prepared, they affirmed that the spin-cast titania films were of a porous nature.[34]

The doping density ($N_D$) of the spray-pyrolyzed $TiO_2$ was determined to be $1.2 \times 10^{17}$ $cm^{-3}$ using a dielectric constant of $\varepsilon_r$ = 54 for $TiO_2$[32] and $R$ = 1.7, which is similar to values reported elsewhere.[32,35] The doping density of FTO ($N_{D,FTO}$) was determined to be $4.1 \times 10^{19}$ $cm^{-3}$ from the slope associated with the space-charge capacitance in the FTO layer using an $\varepsilon_r$ value of 9 for FTO[34] and a value for $R$ of 2.9, which is similar to the values reported by others.[35]

An interesting observation during these measurements was that when comparing the Mott–Schottky measurements on the spray-pyrolyzed $TiO_2$ with a blank FTO sample: the slope associated with the space-charge capacitance of the FTO substrate changed by the same factor (1.7) as the difference in $R_{rms}$ measured with AFM for these two types of substrates. This effect has previously been interpreted as a change in doping density of the FTO layer due to the spray deposition process. We find that this change in slope can be entirely rationalized as being caused by the change in sample surface roughness. We conclude that the surface roughness affects the space-charge capacitance and should be included in the Mott–Schottky relation.[35]

**3.2. Dye Deposition and Dark Characteristics of Solar Cells.** Bilayer solar cell devices were prepared using the small-molecule semiconducting dye TDCV-TPA (structure shown later in Figure 3). The dye layer thickness ($d$) was varied by spin-casting the dye from solution of different concentrations ($c$). The sample absorbance ($A$) was correlated to the effective dye layer thickness $d$ via profilometry measurements of the reference samples on microscope glass slides (see inset of Figure 3). The absorption coefficient at the absorption maximum of TDCV-TPA ($\alpha_{520\ nm}$) was determined to be 3.2 (±0.2) × $10^7$ $m^{-1}$ which is slightly lower than the value we have reported previously[20] but larger than the value reported elsewhere.[36]

For concentrations of $c$ < 5 mM, dye deposition onto the spin-cast titania substrates (Figure 3, blue triangles) resulted in sample absorbances $A$ that were almost twice the value compared to samples prepared on spray-pyrolyzed substrates for the same solution concentration. From the SEM images (Figure 1) and AFM surface topography analysis, we concluded that the spin-cast $TiO_2$ films exhibited a lower surface roughness. Assuming a conformal layer of dye deposited from the same solution concentration, this result was counterintuitive

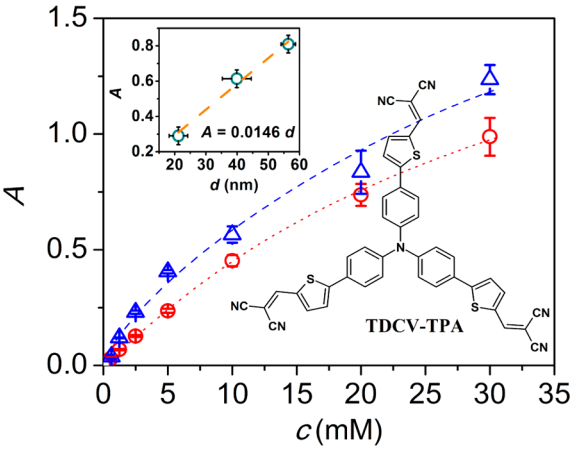


**Figure 3.** Sample absorbance ($A$) at 530 nm in dependency of the solution concentration ($c$) of TDCV-TPA on spray-$TiO_2$ (circles) and spin-$TiO_2$ (triangles) substrates. Trend lines were added as a guide to the eye. Top inset shows the proportionality between $A$ and $d$, derived from Dektak profilometry, and the bottom inset shows the structure of TDCV-TPA.

at first, since more dye would be expected to be deposited onto the spray-pyrolyzed $TiO_2$ substrates. We interpret the relatively larger amount of TDCV-TPA deposited on spin-cast $TiO_2$ substrates as a "soak-in" effect: the small-molecule semiconductor infiltrates the nanoporous spin-cast $TiO_2$ films.

This impression is confirmed by SEM cross-section images of samples prepared with both types of substrates and a dye layer, deposited from a 20 mM solution of TDCV-TPA (see the ESI). In comparison with the absorbance of these samples, the thickness of the dye layer found for the spray-pyrolyzed $TiO_2$ substrates was in the same order as the dye layer visibile in the SEM cross section. For the spin-cast $TiO_2$ layer, we found the thickness of the overstanding TDCV-TPA layer to be ∼17 nm thinner than expected from the sample absorbance. This is another indication that the dye infiltrates the porous $TiO_2$ films prepared by spin-casting.

To analyze the diode properties of the solar cell devices, the dark current density ($J_D$) was measured as a function of applied potential ($V_a$). Figure 4 shows plots of $\ln(|J_D|)$ vs $V_a$ for devices built with both types of $TiO_2$ substrates for various dye layer thicknesses $d$ (indicated in the figure) and reference diodes where the $TiO_2$ layer was directly contacted with PEDOT:PSS ($d$ = 0 nm). The dark diode properties of the solar cell devices was analyzed using a Shockley equation in its logarithmic form, taking both the series $R_s$ and shunt resistance $R_{sh}$ of the solar cell devices into account:[37]

$$\ln(|J_D|) = \ln\left(\frac{R_{sh}}{R_{sh}+R_s}\right) + \ln\left\{j_0\left[\exp\left(\frac{V_a - IR_s}{nk_BT/q}\right) - 1\right] + \frac{V_a}{R_{sh}}\right\} \quad (1)$$

Spray-pyrolyzed titania substrates directly contacted with PEDOT:PSS exhibit $R_{sh}$ on the order of $10^4$ Ω $cm^2$, which increases by 1 order of magnitude when a dye layer is added. The junction formed between the spin-cast titania substrates and PEDOT:PSS exhibit $R_{sh}$ values on the order of $10^3$ Ω $cm^2$ and no rectification. This can be rationalized with short circuits as the $TiO_2$ films prepared by spin-casting are not pinhole-free. These films are thus not suitable to be used as blocking layers in electrochemical and solid-state solar cell devices.

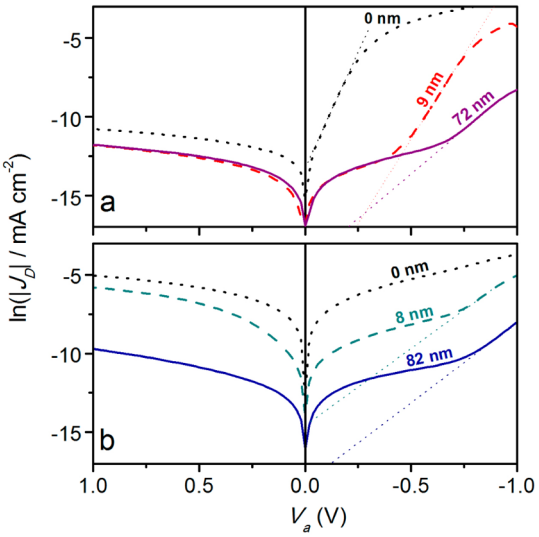


**Figure 4.** Tafel plots of dark current density versus voltage ($J_D$–$V$) of solar cell diodes with varying dye layer thickness $d$ (indicated in Figure) for (a) spray-pyrolyzed $TiO_2$ substrates and (b) spin-cast $TiO_2$ substrates.

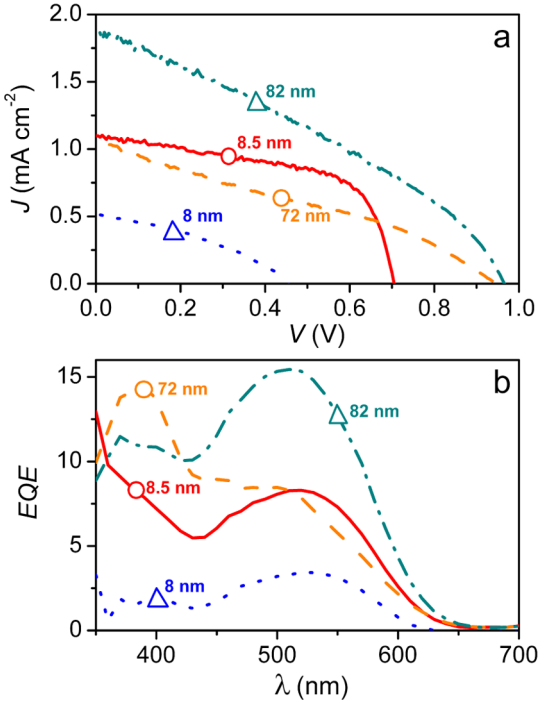


**Figure 5.** (a) Current-density–voltage ($J$–$V$) and (B) EQE spectra of the devices with $d \approx 80$ nm and $d \approx 8$ nm for spin-$TiO_2$ (triangle) and spray-$TiO_2$ (circle). The thickness $d$ is indicated in the figure.

The ideality factor ($n$), the shunt resistance ($R_{sh}$), and the dark exchange current density ($j_0$), which is derived from the dark current density measurements) are compared for both types of substrates and as a function of $d$ in the ESI. The exchange current density ($j_0$) and the ideality factor ($n$) were determined from the extrapolated linear part of the ln $|J_D|$ plot at negative $V_a$. The comparison illustrates that the spray-pyrolyzed $TiO_2$ substrate acts as sufficient blocking layers and rectifying contacts. The spin-cast $TiO_2$ layers exhibit an increase in $R_{sh}$ and decrease in $j_0$ with increasing $d$, which means that the dye layer itself can act as a barrier layer and functioning solar cell diodes can be achieved once the dye layer is thick enough to prevent electrical shorts. The larger variation in the experimental values for the spin-cast substrates reflects that there is a lower reproducibility among individual devices. The larger variance of experimental results for devices prepared with spin-cast $TiO_2$ films shows that these films probably exhibit differences in blocking ability and pinholes between individual samples. Because of their apparently lower adhesion to the underlying FTO substrates, these films might also be more prone to partial destruction during sample preparation.

**3.3. Solar Cells under Illumination.** Current density–voltage ($J$–$V$) measurements under simulated AM1.5 illumination (1000 W $m^{-2}$) were performed to compare the solar energy conversion efficiency ($\eta$) of the two different types of titania substrates. Selected $J$–$V$ curves are shown in Figure 5a for spray-pyrolyzed (circles) and spin-cast (triangles) titania substrates for devices comprising a TDCV-TPA layer with a thickness of ~8 and 80 nm, respectively. In Figure 5b, the corresponding external quantum efficiency (EQE) of these devices is shown.

Bilayer solar cell devices comprising TDCV-TPA and spray-pyrolyzed $TiO_2$ substrates exhibit similar trends in the $J$–$V$ curves and spectral response of the EQE with increasing $d$, as we have discussed previously. In the devices reported herein, the attained power conversion efficiency ($\eta$) was up to 0.47%, which is higher than what we have reported previously.[20] This is due to differences in the batches of TDCV-TPA used. The asymmetric shape of the EQE can be explained with more efficiency harvesting of higher-energy excitons in this device geometry.[20]

For the spin-cast $TiO_2$ substrates devices built with thin layers ($d$ < 20 nm) of TDCV-TPA, the solar cells exhibited short circuits or low device performance. For thicker $d$, the spin-cast $TiO_2$ devices outperformed the devices prepared with spray-pyrolyzed $TiO_2$, reaching efficiencies ($\eta$) up to 0.60% (see the dashed-dotted lines in Figures 5a and 5b).

The improvement in the device performance of HSC devices prepared with spin-cast $TiO_2$ substrates, compared to spray-pyrolyzed $TiO_2$ substrates, stems from a higher generated photocurrent (see Figure 5a). At the absorption maximum, the EQE (Figure 5b) was found to give about twice the response for the spin-cast $TiO_2$ substrates, compared to spray-pyrolyzed samples.

Considering the more porous nature of the spin-cast $TiO_2$ substrates, as apparent from SEM analysis (Figure 1b) and the soak-in effect observed for the dye deposition (Figure 3), we interpret the higher photocurrent to be a consequence of a larger interfacial area for charge separation. Comparing the SEM cross-sections of samples with deposited TDCV-TPA, we found that for the spin-cast $TiO_2$ films the overstanding TDCV-TPA layer was ~17 nm thinner than expected from the sample absorbance (see the ESI). This corresponds to ~72% of the light harvested in the interpenetrated dye/$TiO_2$ region. Since the distance to the nearest $TiO_2$ interface can be expected to be small, excitons are harvested very efficiently.

The spectral response of the solar cell devices appears significantly different for devices comprising spin-cast and spray-pyrolyzed $TiO_2$ substrates for thick TDCV-TPA layers (Figure 5b). The mismatch between the EQE of TDCV-TPA and the corresponding light harvesting efficiency (LHE) of the device has been observed previously and is due to a more-efficient exciton harvesting for the higher-energy excitons in


dx.doi.org/10.1021/am301604x | ACS Appl. Mater. Interfaces 2012, 4, 5997–6004

TDCV-TPA created at 380 nm.[20] This effect is only apparent if the dye layer thickness can exceed the exciton diffusion length ($L_{XD}$) for the lower energy transition. The lack of the distortion of the EQE spectrum for devices built with the spin-cast $TiO_2$ substrates indicates that excitons are generated within the $L_{XD}$ of the lower-energy excitons. We interpret this to be due to exciton harvesting in TDCV-TPA infiltrated into the nanoporous spin-cast $TiO_2$ films where the average distance to an interface would be on the order of the exciton diffusion length.

The effect of the preparation route of the titania might be negligible in comparable HSC devices comprised of polymers.[8,23] To our knowledge, a systematic comparison of $TiO_2$ substrates prepared using different preparation routes has not been reported for polymer/titania HSC devices.

The efficiencies for the bilayer devices comprising TDCV-TPA and spin-cast $TiO_2$ films reported herein compare favorably with bilayer HSCs using $TiO_2$ films prepared in a similar manner in combination with poly-3-hexylthiophene.[8] TDCV-TPA is thus an interesting compound to be used in HSC devices and the smaller molecular dimensions might prove to be beneficial when realizing nanostructured HSCs, because the dimensions of the organic compound affect the infiltration into the scaffold of a porous inorganic acceptor.[27]

In Figure 6, the $d$-dependency of the EQE, the open-circuit voltage ($V_{OC}$), and the fill factor (FF) are compared for all devices investigated in this study. From the $d$-dependency of the EQE, the exciton diffusion length ($L_{XD}$) can be determined.[20,38] For the spin-cast $TiO_2$ substrates, we found no systematic dependence of the EQE on the dye layer thickness $d$, because devices with thin $d$ were not functional.

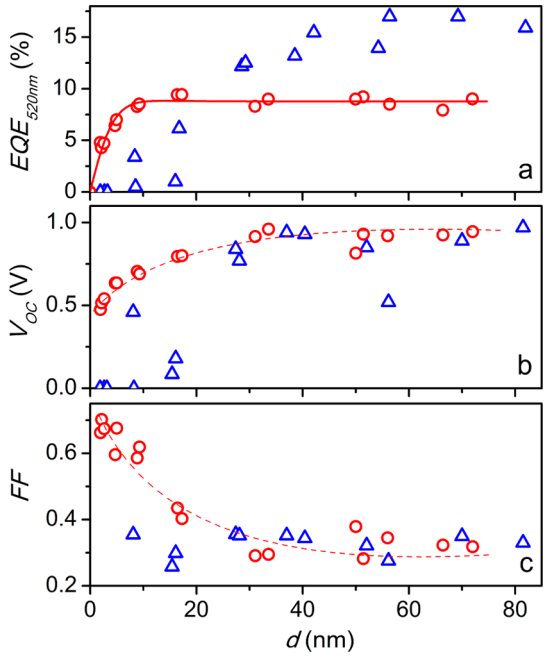


**Figure 6.** Comparison of (a) the external quantum efficiency (EQE) at absorption maximum of TDCV-TPA (520 nm), (b) the open-circuit voltage $V_{OC}$, and (c) the fill factor (FF), with regard to their dependency of the dye layer thickness $d$ for hybrid solar cell (HSC) devices prepared with spray-pyrolyzed (circles) and spin-cast (triangles) $TiO_2$ substrates. Trend lines in the $d$-dependence of $V_{OC}$ (panel (b)) and FF (panel (c)) were added as a guide to the eye. For the spray-pyrolyzed $TiO_2$ substrates, the EQE dependency on $d$ could be fit to an exciton diffusion model.

However, the analysis could be carried out for the spray-pyrolyzed titania substrates.

The $L_{XD}$ value of TDCV-TPA was determined to be 6.5 nm for an interfacial charge transfer efficiency ($\eta_{CT}$) of 52%, assuming a nonquenching PEDOT:PSS interface and planar interfaces (fit to $d$-dependent EQE data in Figure 6a). Assuming a quenching PEDOT:PSS contact and allowing for $\eta_{CT}$ = 100%, the $L_{XD}$ value was determined to be 3.3 nm. This is slightly higher than that reported previously,[20] which is partially due to the different absorption coefficient used in this study but also is due to the higher overall performance of the devices. The exciton diffusion models employed assume planar interfaces which, as we have shown here, is not necessarily a valid assumption. Considering the surface roughness of the spray-pyrolyzed titania substrates, these values are an overestimation as the distance to the nearest interface could be smaller than the dye layer thickness $d$ derived from the optical absorbance.

The $V_{OC}$ values (Figure 6b) exhibited a similar $d$-dependency for the devices built with spray-pyrolyzed $TiO_2$ substrates, as reported previously.[20] The shift in the $V_{OC}$ and voltage onset in darkness (Figure 5a) can be rationalized with TDCV-TPA acting as a dielectric layer between the two electric contacts. The spin-cast substrates exhibited short circuits for thin dye layers. At thicker $d$, the $V_{OC}$ appears to reach a limiting value of 0.95 V for both types of substrates. As in organic solar cells, the $V_{OC}$ value in HSC devices is expected to be limited by the difference in the quasi-Fermi level $E_{F,n}$ for electrons in the $n$-type $TiO_2$ and the quasi Fermi level $E_{F,p}$ for holes in TDCV-TPA. For thin dye layers, however, the $V_{OC}$ is influenced by the contact between $TiO_2$ and PEDOT:PSS and the limiting $V_{OC}$ can only be established for dye layers thick enough to prevent a direct contact between $TiO_2$ and PEDOT:PSS efficiently. At low dye coverage, the $V_{fb}$ in $TiO_2$ might also be influenced by the acidity of PEDOT:PSS.[39] The similar limiting $V_{OC}$ value for both types of $TiO_2$ substrates supports the hypothesis that the $V_{fb}$ of the titania films is similar for both types of substrates.

The fill factor (FF) for the spray-pyrolyzed $TiO_2$ substrates was found to decrease from ~0.7 to ~0.3 with increasing $d$. This was previously rationalized with a limitation in the hole transport through the TDCV-TPA layer with increasing $d$.[20] For the spin-cast $TiO_2$ layers, the FF is ~0.3, even for small $d$. This can be ascribed to higher recombination losses, which is also apparent in the low shunt resistance ($R_{sh}$) and dark saturation current density ($j_0$) observed in the dark $J-V$ measurements (see Figure 4b).

Photovoltage ($V_{OC}$) decay measurements were carried out to gain insight into the recombination processes in the solar cell devices. After illumination for 10 s with an LED with an approximate light intensity of 1 sun, the light source was switched off and the voltage decay was recorded over time. In Figure 7, the $V_{OC}$ decay for devices built with the spin-cast $TiO_2$ (triangles) and spray-pyrolyzed $TiO_2$ substrates (circles) is shown in a semilogarithmic plot.

The voltage decay was found to be multiexponential. In the devices investigated herein, up to four recombination pathways must be considered, as indicated in the energy level diagram (see Figure 7, inset). Process (1) is the recombination of electrons in $TiO_2$ with holes in the dye layer and process (2) is the recombination of electrons in $TiO_2$ with holes in PEDOT:PSS. If the titania layer is not sufficiently blocking the FTO, pathways (3) and (4), which are recombination

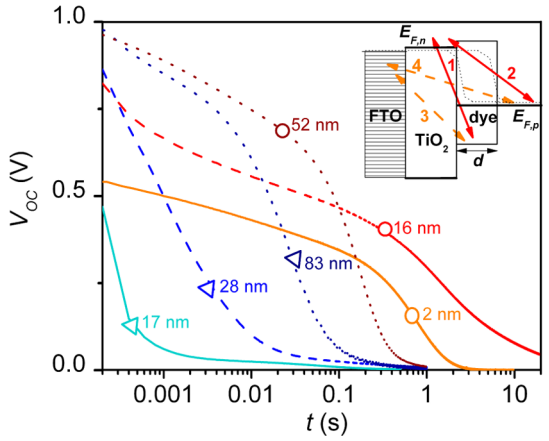


**Figure 7.** Photovoltage ($V_{OC}$) decay for bilayer devices using spin-cast $TiO_2$ (triangles) and spray-pyrolyzed $TiO_2$ (circles) substrates and various dye layer thickness (indicated in figure). Inset shows an illustration of recombination pathways at the different interfaces in the solar cell device.

processes via interfaces of either the dye or PEDOT:PSS with the FTO substrate, must be considered.

Devices built with spin-cast $TiO_2$ substrates exhibit faster $V_{OC}$ decays on shorter time scales compared to devices built with spray-pyrolyzed $TiO_2$ substrates. For thin $d$, no considerable device voltage was measurable, since all charges were lost rapidly through recombination. With increasing $d$, the recombination kinetics of the spin-cast titania devices become slower. This is another indication that the dye layer acts as a barrier between the FTO and PEDOT:PSS interfaces. For thicker dye layers, we could therefore build functioning solar cell devices with the spin-cast titania substrates that even exceeded the performance of devices built with spray-pyrolyzed $TiO_2$.

For the devices built with spray-pyrolyzed $TiO_2$ substrates, the $V_{OC}$ decay occurred on a longer time scale. In these devices, recombination pathways to the FTO (pathways 3 and 4 in the inset of Figure 7) can be neglected. Increasing the dye layer from thin layers to $d \approx 20$ nm, the $V_{OC}$ decay becomes slower, indicating that recombination events become less frequent with increasing dye layer thickness. We interpret the faster $V_{OC}$ decay for $d > 40$ nm to be due to a less-sufficient extraction of photogenerated holes from the TDCV-TPA layer.

## 4. CONCLUSIONS

In bilayer hybrid solar cells (HSCs), the device performance depends critically on the nanoscale morphology of the interface between the inorganic and organic semiconducting components. Herein, we investigated two different routes for the preparation of flat titanium dioxide layers, $TiO_2$, as the inorganic component in bilayer HSCs in combination with the small-molecule semiconductor TDCV-TPA as the organic component.

The preparation routes investigated were spray pyrolysis and spin-casting of a $TiO_2$ precursor. Both preparation routes result in anatase $TiO_2$ films, consisting of crystallites in the order of 25 nm and with similar optical and electronic properties. The investigated $TiO_2$ films exhibited big differences in film morphology, and electrochemical measurements proved that spin-cast $TiO_2$ films were not dense. In addition, we found that the small-molecule semiconductor TDCV-TPA infiltrated the spin-cast $TiO_2$ substrates. We concluded that the spin-cast preparation route results in nanoporous $TiO_2$ films.

Both in electrochemical measurements and the investigated solar cell diodes, spray-pyrolyzed $TiO_2$ layers were found to be blocking the underlying FTO substrates. The spin-cast $TiO_2$ films exhibited pinholes, which resulted in short circuits in devices built with spin-cast $TiO_2$ substrates when only a thin layer of TDCV-TPA was present. In devices with thicker $d$, the dye layer acts as a barrier, preventing recombination losses to the FTO substrate.

Because of the nanoporosity of the spin-cast $TiO_2$ layers, bilayer solar cells prepared with these substrates exhibited higher photocurrents, due to a more efficient exciton harvesting. Power conversion efficiencies up to 0.60% were observed, while devices built with spray-pyrolyzed titania films gave up to 0.47%. Small-molecule semiconductors with high absorption coefficients, such as TDCV-TPA, are interesting for the development of nanostructured HSCs, because of a facile infiltration into nanostructured inorganic networks.

## ■ ASSOCIATED CONTENT

### Supporting Information

Additional SEM images; AFM of FTO substrate; X-ray diffraction data; Transmittance and reflectance spectra; Photoelectron spectroscopy data; Electrochemical measurements; Parameters from dark J-V fits. This material is available free of charge via the Internet at http://pubs.acs.org.

## ■ AUTHOR INFORMATION

### Corresponding Author

*Tel.: +46-184713303. Fax: +46-184713633. E-mail: Gerrit.Boschloo@kemi.uu.se.

### Present Addresses

[∇]McCullough Building, 476 Lomita Mall, Stanford University, Stanford, CA 94305 USA. E-mail: eunger@stanford.edu.

[⊥]50 Nanyang Drive, Research Techno Plaza, Energy Research Insitute at NTU, Singapore, 637553.

[○]VG Scienta AB, P.O. Box 15120, SE-750 15 Uppsala, Sweden.

### Author Contributions

The manuscript was written through contributions of all authors. All authors have given approval to the final version of the manuscript.

### Notes

The authors declare no competing financial interest.

## ■ ACKNOWLEDGMENTS

We thank the Swedish Research Council (VR), the Swedish Energy Agency and the STandUP for energy program for financial support. We thank Jesper Jakobsson, Jonathan Scragg, and James Gardner (Uppsala University) for useful discussions and advice. The staff at MAX-lab in Lund, Sweden is thanked for competent and friendly assistance during the PES measurements.

## ■ REFERENCES

(1) Günes, S.; Sariciftci, N. S. *Inorg. Chim. Acta* **2008**, *361*, 581−588.
(2) Bouclé, J.; Ravirajan, P.; Nelson, J. *J. Mater. Chem.* **2007**, *17*, 3141−3153.
(3) Bach, U.; Lupo, D.; Comte, P.; Moser, J. E.; Weissortel, F.; Salbeck, J.; Spreitzer, H.; Grätzel, M. *Nature* **1998**, *395*, 583−585.
(4) Coakley, K. M.; McGehee, M. D. *Appl. Phys. Lett.* **2003**, *83*, 3380−3382.

(5) Mor, G. K.; Kim, S.; Paulose, M.; Varghese, O. K.; Shankar, K.; Basham, J.; Grimes, C. A. *Nano Lett.* **2009**, *9*, 4250−4257.
(6) Oosterhout, S. D.; Wienk, M. M.; van Bavel, S. S.; Thiedmann, R.; Jan Anton Koster, L.; Gilot, J.; Loos, J.; Schmidt, V.; Janssen, R. A. J. *Nat. Mater.* **2009**, *8*, 818−824.
(7) Ravirajan, P.; Peiro, A. M.; Nazeeruddin, M. K.; Grätzel, M.; Bradley, D. D. C.; Durrant, J. R.; Nelson, J. *J. Phys. Chem. B* **2006**, *110*, 7635−7639.
(8) Goh, C.; Scully, S. R.; McGehee, M. D. *J. Appl. Phys.* **2007**, *101*, 114503.
(9) Lira-Cantu, M.; Krebs, F. C. *Sol. Energy Mater. Sol. Cells* **2006**, *90*, 2076.
(10) Savenije, T. J.; Warman, J. M.; Goossens, A. *Chem. Phys. Lett.* **1998**, *287*, 148−153.
(11) Gregg, B. A. *J. Phys. Chem. B* **2003**, *107*, 4688−4698.
(12) Karthikeyan, C. S.; Thelakkat, M. *Inorg. Chim. Acta* **2008**, *361*, 635−655.
(13) Daeneke, T.; Kwon, T.-H.; Holmes, A. B.; Duffy, N. W.; Bach, U.; Spiccia, L. *Nature Chem.* **2010**, *3*, 211−215.
(14) Feldt, S. M.; Gibson, E. A.; Gabrielsson, E.; Sun, L.; Boschloo, G.; Hagfeldt, A. *J. Am. Chem. Soc.* **2010**, 16714−16724.
(15) Conings, B.; Baeten, L.; Boyen, H.-G.; D'Haen, J.; Van Bael, M. K.; Manca, J. V. *J. Phys. Chem. C* **2012**, *116*, 14237−14242.
(16) Daoud, W. A.; Turner, M. L. *React. Funct. Polym.* **2006**, *66*, 13.
(17) Breeze, A. J.; Schlesinger, Z.; Carter, S. A.; Tillmann, H.; Hörhold, H. H. *Sol. Energy Mater. Sol. Cells* **2004**, *83*, 263−271.
(18) Scully, S. R.; McGehee, M. D. *J. Appl. Phys.* **2006**, *100*, 034907.
(19) Skotheim, T.; Yang, J. M.; Otvos, J.; Klein, M. P. *J. Chem. Phys.* **1982**, *77*, 6144−6150−6161.
(20) Unger, E. L.; Ripaud, E.; Leriche, P.; Cravino, A.; Roncali, J.; Johansson, E. M. J.; Hagfeldt, A.; Boschloo, G. *J. Phys. Chem. C* **2010**, *114*, 11659−11664.
(21) Liu, Y.; Summers, M. A.; Edder, C.; Fréchet, J. M. J.; McGehee, M. D. *Adv. Mater.* **2005**, *17*, 2960−2964.
(22) Kavan, L.; Grätzel, M. *Electrochim. Acta* **1995**, *40*, 643−652.
(23) Arango, A. C.; Johnson, L. R.; Bliznyuk, V. N.; Schlesinger, Z.; Carter, S. A.; Hörhold, H. H. *Adv. Mater.* **2000**, *12*, 1689−1692.
(24) Cravino, A.; Roquet, S.; Alévêque, O.; Leriche, P.; Frère, P.; Roncali, J. *Chem. Mater.* **2006**, *18*, 2584−2590.
(25) Roquet, S.; Cravino, A.; Leriche, P.; Alévêque, O.; Frère, P.; Roncali, J. *J. Am. Chem. Soc.* **2006**, *128*, 3459−3466.
(26) McGehee, M. D. *MRS Bull.* **2009**, *34*, 95−100.
(27) Johansson, E. M. J.; Pradhan, S.; Wang, E.; Unger, E. L.; Hagfeldt, A.; Andersson, M. R. *Chem. Phys. Lett.* **2011**, *502*, 225−230.
(28) Horcas, I.; Fernandez, R.; Gomez-Rodriguez, J. M.; Colchero, J.; Colchero, J.; Gomez-Herrero, J.; Baro, A. M. *Rev. Sci. Instrum.* **2007**, *78*, 013705.
(29) Bässler, M.; Forsell, J. O.; Björneholm, O.; Feifel, R.; Jurvansuu, M.; Aksela, S.; Sundin, S.; Sorensen, S. L.; Nyholm, R.; Ausmees, A.; Svensson, S. *J. Electron. Spectrosc.* **1999**, *101−103*, 953−957.
(30) Svensson, S.; Forsell, J. O.; Siegbahn, H.; Ausmees, A.; Bray, G.; Södergren, S.; Sundin, S.; Osborne, S. J.; Aksela, S.; Nommiste, E.; Jauhiainen, J.; Jurvansuu, M.; Karvonen, J.; Barta, P.; Salaneck, W. R.; Evaldsson, A.; Lögdlund, M.; Fahlman, A. *Rev. Sci. Instrum.* **1996**, *67*, 2149−2156.
(31) Viseu, T. M. R.; Almeida, B.; Stchakovsky, M.; Drevillon, B.; Ferreira, M. I. C.; Sousa, J. B. *Thin Solid Films* **2001**, *401*, 216−224.
(32) van de Krol, R.; Goossens, A.; Schoonman, J. *J. Electrochem. Soc.* **1997**, *144*, 1723−1727.
(33) Boschloo, G. K.; Goossens, A.; Schoonman, J. *J. Electrochem. Soc.* **1997**, *144*, 1311−1317.
(34) Fabregat-Santiago, F.; Garcia-Belmonte, G.; Bisquert, J.; Bogdanoff, P.; Zaban, A. *J. Electrochem. Soc.* **2003**, *150*, E293−E298.
(35) Cameron, P. J.; Peter, L. M. *J. Phys. Chem. B* **2003**, *107*, 14394−14400.
(36) Sulaiman, K.; Fakir, M. S. *Thin Solid Films* **2011**, *519*, 5219−5222.
(37) Huynh, W. U.; Dittmer, J. J.; Teclemariam, N.; Milliron, D. J.; Alivisatos, A. P.; Barnham, K. W. J. *Phys. Rev. B* **2003**, *67*, 115326.
(38) Kroeze, J. E.; Savenije, T. J.; Vermeulen, M. J. W.; Warman, J. M. *J. Phys. Chem. B* **2003**, *107*, 7696−7705.
(39) Watson, D. F.; Marton, A.; Stux, A. M.; Meyer, G. J. *J. Phys. Chem. B* **2003**, *107*, 10971−10973.